Molecular Dynamics Study of Water Adsorption on TiO2 Nanoparticles

ARTICLE *in* THE JOURNAL OF PHYSICAL CHEMISTRY C · MAY 2007

Impact Factor: 4.77 · DOI: 10.1021/jp0666380

2 AUTHORS:

Vishal N Koparde
Virginia Commonwealth University
18 PUBLICATIONS **213** CITATIONS
SEE PROFILE

Peter T Cummings
Vanderbilt University
518 PUBLICATIONS **11,778** CITATIONS
SEE PROFILE

ARTICLES

Molecular Dynamics Study of Water Adsorption on TiO_2 Nanoparticles

Vishal N. Koparde* and Peter T. Cummings

Department of Chemical Engineering, Vanderbilt University, VU Station B 351604, Nashville, Tennessee 37235

Received: October 9, 2006; In Final Form: March 15, 2007

This study uses molecular dynamics simulations performed in a parallel computing environment to investigate the adsorption of water molecules on the surface of anatase and rutile nanoparticles ranging from 2.5 to 4 nm at room temperature and at hydrothermal conditions. Phase enhancement occurs when these nanoparticles are immersed in water and the coverage per unit area of the nanoparticles increases with increase in size. The residence time of water molecules at the nanoparticle surface is ∼5−6 times longer at room temperature than that under hydrothermal conditions. Examining the oxygen and hydrogen atom distribution from the nanoparticle surfaces, it is found that there are two hydration layers around all the nanoparticles under consideration at all conditions. In the first hydration layer, water molecules have two different simultaneously existing orientational preferences depending on their local environment.

Introduction

As the size of particles decreases their properties change dramatically. Hence, when one of the dimensions of condensed matter is in the nanometer range, its properties are significantly different than the bulk. This change in physical and chemical properties of materials when in the nanometer range has greatly intrigued researchers in recent decades.[1−4] Due to its unique behavior, nanoscaled condensed matter has been finding novel application in the fields of electronics,[5] aerospace,[6] electrochemistry,[7] and medicine.[8,9] One example is titanium dioxide, a widely occurring metal−oxide semiconductor. Due to its opacity, it has been used as a white pigment in paints[10−13] and papers; however, nowadays, nanosized titania is widely used as a raw material in electronic and structural ceramics.[14] It is also used in dye-sensitized solar cells and in high-temperature separation and photocatalytic applications.[11,15−18] Recently, nanosized titania has been used as a catalyst in many different reactions under ultraviolet light, such as alcohol dehydration,[19] degradation of paint pigments,[20] oxidation of aromatic compounds,[21] nitrogen oxide reduction,[22] and removal of toxic contaminants from wastewater.[16,17]

Titanium dioxide has been reported in the literature to exist in seven known polymorphs.[23] Anatase, rutile, and brookite are the most abundant in nature.[15,24−26] The crystals of brookite are orthorhombic, while anatase and rutile are tetragonal.[13,15,24,27] Rutile has been found to be the most stable polymorph in the bulk form. Bulk anatase and brookite transform irreversibly and exothermically to rutile when subjected to heat.[23,28−30] Nanosized titania is manufactured by two processes, namely, the dry process[31,32] or the "chloride" process and the wet process.[13,33] In the dry process, titanium dioxide is prepared by direct oxidation of titanium tetrachloride in a flame reactor at high temperature and low pressure. In the wet process, titanium dioxide nanoparticles are prepared in aqueous environment and the water is usually at hydrothermal conditions. Hence, we have chosen a temperature of 523 K and a pressure of 50 kbar for the majority of our simulations. The motivation behind this research work is to understand the behavior of water molecules near the surface of titanium dioxide nanoparticles and the variation of their thermodynamic, structural, and transport properties with nanoparticle size and environmental conditions. As rutile and anatase are more important polymorphs of TiO_2 due to their numerous applications, we have not considered brookite in our study. The extremely small size of these particles makes them ideal candidates for investigation with molecular dynamics (MD) simulation, which has been a long-established simulation technique to extensively investigate structural and dynamic properties of solids and fluids at the atomic scale.

Simulation Details

Force Fields. A large number of force fields have been reported in the literature for modeling TiO_2 polymorphs.[34−43] A detailed survey of most of these force fields has been published elsewhere by Collins and co-workers.[44] It can be concluded from their report that the Matsui−Akaogi force field[40] is the most suitable for classical molecular dynamics simulations of bulk titanium dioxide polymorphs for a wide range of temperatures. It has also been found[45] that the Matsui−Akaogi force field outperforms a more complex variable charge force field that involves greater computational cost. The Matsui−Akaogi force field reproduces the structures of four TiO_2 polymorphs and their order of relative stabilities when compared to limited experimental data.[44] Also, it is a two-body rigid-ion potential with a simpler and computationally less demanding analytical form. Clearly, surface effects are extremely important when studying nanoparticles. Bandura and Kubicki[46] have verified the suitability of using the Matsui−Akaogi force field to study rutile surfaces, using various quantum mechanical methods. Hence, we have chosen the Matsui−Akaogi force field to model TiO_2 nanoparticles in this work. Thus, the site−site

* Address correspondence to this author.

10.1021/jp0666380 CCC: $37.00
Published on Web 04/24/2007

TABLE 1: Interaction Parameters for the Matsui−Akaogi Force Field[47]

interaction	A_{ij}, kcal mol^{-1}	ρ_{ij}, Å	C_{ij}, kcal mol^{-1} Å^{-6}
Ti−Ti	717654	0.154	120.997
Ti−O	391053	0.194	290.392
O−O	271719	0.234	696.941

TABLE 2: Number of TiO_2 Units and Number of Water Molecules in Each Simulation Box

particle	no. of TiO_2 units	no. of water molecules
2.5 nm anatase	228	1605
2.5 nm rutile	257	1598
3.0 nm anatase	417	2757
3.0 nm rutile	491	2756
3.5 nm anatase	656	4367
3.5 nm rutile	718	4363
4.0 nm anatase	979	6552
4.0 nm rutile	1073	6550

TABLE 3: SPC/E Parameters[46]

$i-j$	ϵ_{ij} (kcal/mol)	σ_{ij} (Å)
O_W-O_W	0.15539	3.5532
O_W-H_W	0.000	
H_W-H_W	0.000	

interactions between Ti and O ions in the nanoparticles can be represented as[47]

$$U(r_{ij}) = A_{ij}\exp\left(-\frac{r_{ij}}{\rho_{ij}}\right) - \frac{C_{ij}}{r_{ij}^{6}} + \frac{q_i q_j}{r_{ij}} \qquad (1)$$

where $U(r_{ij})$ is the interaction energy between sites i and j, r_{ij} is the distance between them, and the parameters A_{ij}, ρ_{ij}, and C_{ij} are listed in Table 1. The Ti and O ions have partial charges (q) of +2.196 and −1.098, respectively.

The SPC/E[48] potential is used to model water molecules around the TiO_2 nanoparticles. It is a three-site model with one negatively ($q_{OW} = -0.8476$) and two positively ($q_{HW} = +0.4238$) charged sites representing the O and H atoms in the water molecule, respectively. It can be written as

$$U(r_{ij}) = \epsilon_{ij}\left[\left(\frac{\sigma_{ij}}{r_{ij}}\right)^{12} - 2\left(\frac{\sigma_{ij}}{r_{ij}}\right)^{6}\right] + \frac{q_i q_j}{r_{ij}} \qquad (2)$$

The values of the parameters are listed in Table 3. Note that in this form of the LJ potential the parameter σ_{ij} is the distance at which the LJ potential has its minimum value of $-\epsilon_{ij}$. To model the interactions between the water molecules and the nanoparticles we have used the ab initio derived interaction parameters reported by Bandura and Kubicki.[46]

Simulation Method. Constant temperature and constant pressure MD simulations where carried out with use of the Daresbury laboratories' MD code, DLPOLY[49,50] version 2.13. The Nosé-Hoover thermostat and barostat are applied to all the species in the simulation box to maintain their temperature and pressure, respectively. DLPOLY uses Verlet's leapfrog algorithm in conjunction with the multiple time step method to integrate Newton's laws of motion over time. Each simulation considers a simulation box, which has periodic boundaries in the *x*-, *y*-, and *z*-directions. The size of the box was chosen such that the interaction between the particle and its own image in the neighboring box is negligible. This is ensured by choosing the side of the cubic box to be 24 Å larger than the diameter of the particle. Thus, the surface-to-surface distance between a nanoparticle and its own periodic image is about 24 Å. The temperature of 523 K and pressure of 50 kbar are chosen for simulating hydrothermal conditions (HT). For the simulations at room temperature and pressure (ambient), the values of 300 K and 1 bar are used. The simulations are repeated for rutile and anatase nanoparticles of 2.5, 3, and 4 nm diameters. The number if TiO_2 units and the number of water molecules in each simulation box is reported in Table 2. The procedure to make the initial configurations of the nanoparticles is identical with the procedure reported in our earlier publication.[51] The *wateradd* utility of DL_POLY is used to add SPC/E water molecules to the simulation box. For all simulations a time step of 0.5 fs is used and statistical data are collected every 2000 time steps. After an equilibration period of 250 ps, data production runs of 750 ps are conducted for all the simulations.

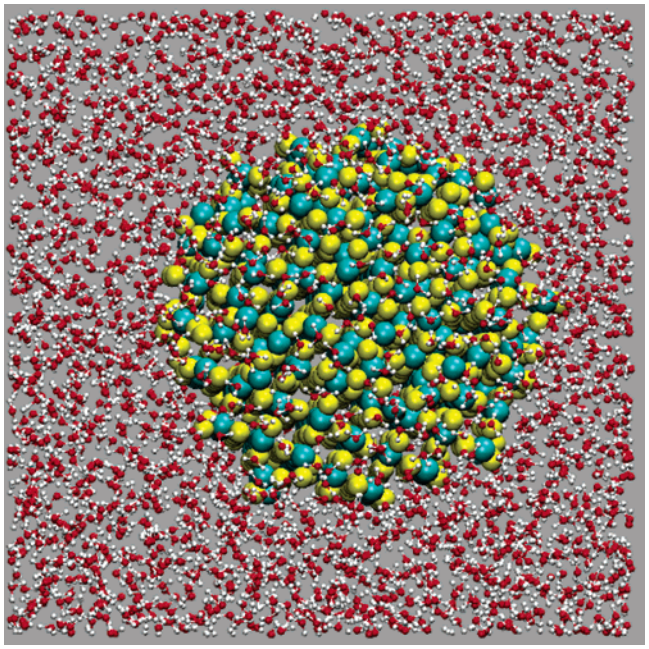

Figure 1. Snapshot of a 3 nm rutile nanoparticle in water (Ti, cyan; O, yellow; water, red/white).

Results and Discussion

Figure 1 gives a snapshot of a 3 nm rutile nanoparticle surrounded by water molecules. The simulation box contains 491 TiO_2 units, each containing one Ti and two O ions, and 2756 water molecules, each containing one O and two H atoms. Figure 2 compares the simulated X-ray diffraction patterns of rutile nanoparticles in vacuum, under hydrothermal conditions (HT), and at room temperature and pressure (ambient). The simulated X-ray diffraction patterns were determined by using Debye functional analysis as described by Kazakov and coworkers.[52] The details about this procedure are reported by Naicker et al.[47] These simulated X-ray diffraction patterns suggest that the nanoparticles do not undergo any phase transformations when immersed in water at HT or ambient conditions. The rutile 110 X-ray diffraction peak, observed at $2\theta = 27.5°$, is taller for the particles immersed in water than those in vacuum. It should be noted that vacuum simulations were carried out at a constant temperature of 300 K. Also, the height of the rutile 220 peak ($2\theta = 55°$) is higher for a particle at ambient conditions than that particle in a hydrothermal environment, which is in turn higher than that for a particle in vacuum. This suggests that when TiO_2 nanoparticles are immersed in water they undergo some degree of structural change. The nanoparticles in water at ambient conditions are

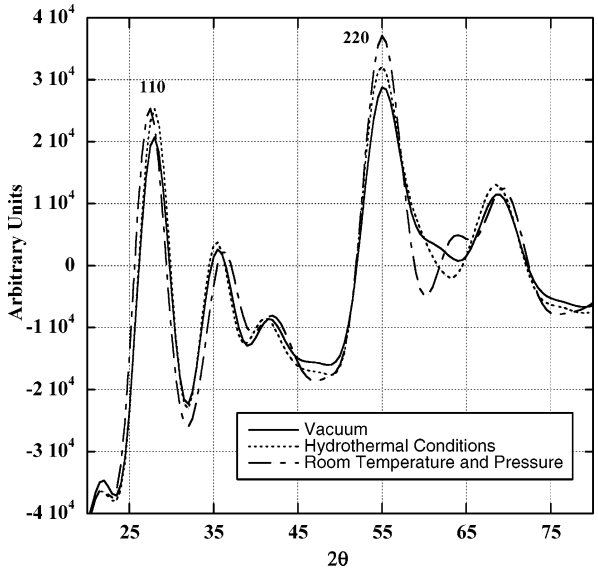

Figure 2. Simulated X-ray diffraction patterns of a 3 nm rutile nanoparticle in vacuum, under hydrothermal conditions and at room temperature and pressure.

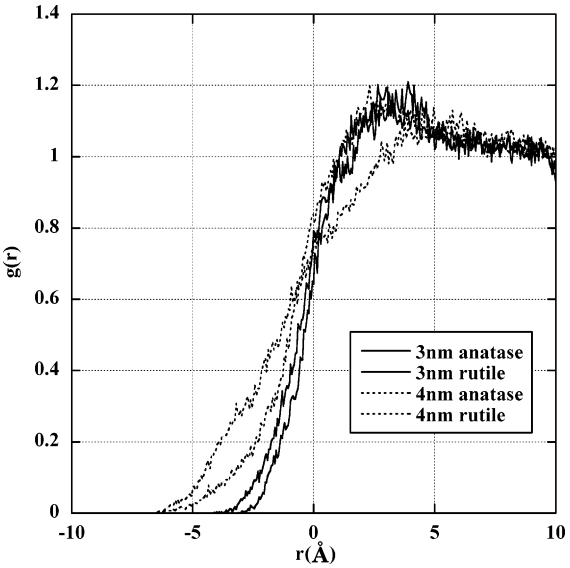

Figure 3. Water density profiles around 3 and 4 nm anatase and rutile nanoparticles under hydrothermal condtions.

TABLE 4: Coordination Number Distribution of a 2.5 nm Rutile Nanoparticle

coordination no.	% in vacuum	% at HT	% at ambient conditions
3	0.01	1.48	1.75
4	11.06	12.73	11.51
5	31.81	25.21	26.93
6	56.75	60.17	59.79
7	0.38	0.41	0.02

more crystalline than those in water at HT, which are more crystalline than those in vacuum. Table 4 shows the percentage distributions of coordination numbers of Ti ions in 2.5 nm rutile particles under various conditions. The coordination number of a Ti ion is defined as the average number of O ions within a sphere of radius 2.5 Å around it. The table shows that the percentages of 3, 4, and 7 coordinated Ti ions are relatively small in all cases. This is also found to be true of all other simulations. After examining the coordination number distributions of anatase and rutile nanoparticles ranging from 2.5 to 4 nm, we found that about 5% of Ti ions, which were 5-coordinated in vacuum, are 6-coordinated when immersed in water. It should be noted that the coordination between Ti ions and the O atoms in the water molecules is not considered while calculating these coordination numbers for the Ti ions, in order to make them comparable to the vacuum calculations. This corroborates our previous conclusion that the nanoparticles are more crystalline in water than in vacuum. Zhang and coworkers[53] also report similar conclusions for ZnS nanoparticles in the same size range.

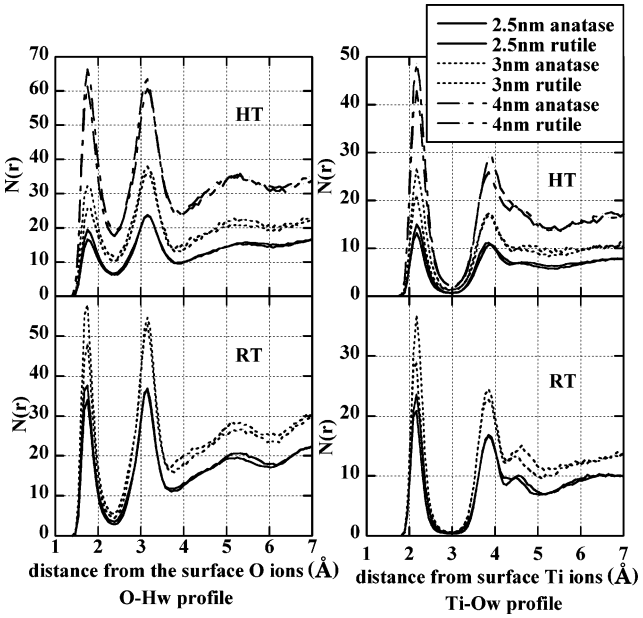

Figure 4. Water profiles around different sizes of anatase and rutile nanoparticles under hydrothermal conditions and at ambient conditions calculated with respect to surface ions.

Density Profiles. Figure 3 shows the density profile of water at HT around the nanoparticle, with respect to the center of mass of the particle. There is no significant increase in water density around the particles suggesting that the particles are not hydrophilic. The broadness of the density peak is due to the fact that the surface of the nanoparticle is very rough. Hence, the density profile determined with respect to the center of mass of the nanoparticle cannot be compared to the water density profile near a planar surface. In fact, these profiles cannot be compared with each other with confidence as the surface roughness of the nanoparticles may vary from particle to particle.

To better understand the arrangement of water molecules near the nanoparticle surface and to overcome the problem of surface roughness, we determine the water density with respect to the surface ions. Figure 4 shows the number of water oxygens when calculated from the outermost Ti ions on the nanoparticle surface and the number of water hydrogens calculated from the outermost O ions on the nanoparticle surface. Two distinct peaks of water oxygens are observed at 2.1 and 3.9 Å, respectively. These values are comparable to the water oxygen peaks observed at 2.2 and 3.7−3.8 Å from a bare nonhydroxylated rutile (110) surface.[54] For all sizes of nanoparticles considered, the first peak for rutile is taller than the first peak for anatase and the second peak for anatase is taller than the second peak for rutile, in both ambient and hydrothermal conditions. This suggests that the surface Ti ions of rutile attract water oxygens stronger than their anatase counterparts.

Similarly in the hydrogen profiles, two significant peaks are observed at 1.8 and 3.1 Å from the surface O ions. Again, the first peak is taller for rutile and the second peak is taller for anatase particles of the same size. Since the relative positions

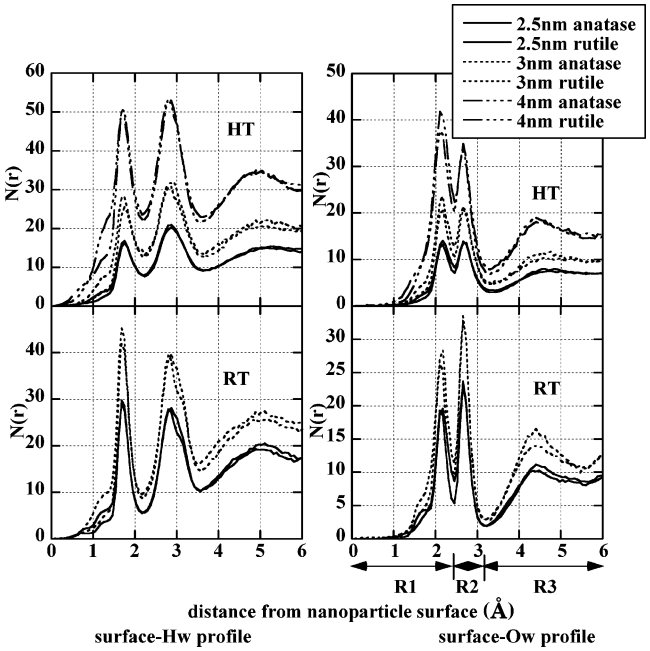

Figure 5. Water profiles around different sizes of anatase and rutile nanoparticles under hydrothermal conditions and at ambient conditions calculated from the surface defined by surface ions.

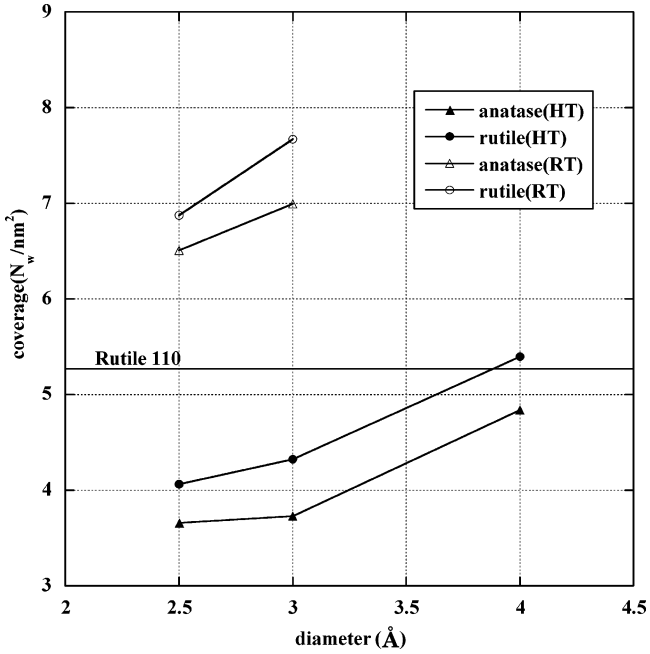

Figure 6. Number of water molecules per unit surface area (water coverage) for various sizes of anatase and rutile nanoparticles at hydrothermal conditions and at ambient conditions.

of the surface Ti and O ions vary considerably across the rough nanoparticle surface, we cannot directly superimpose the oxygen and hydrogen profiles. To achieve this, we had to determine the water distribution profile from the nanoparticle surface without biasing between the surface Ti and O ions. Hence, we determined the three nearest surface ions (denoted as A, B, and C) from each water molecule, and then calculated the minimum distance between the water molecules and the triangle defined by these three ions, referred to subsequently as the triangle ABC. Using these distances we plot the water distribution profiles shown in Figure 5. The ordering of water molecules is prominent only in the first 6 Å from the nanoparticle surface, beyond which the oscillations quickly damp out. In all simulations, independent

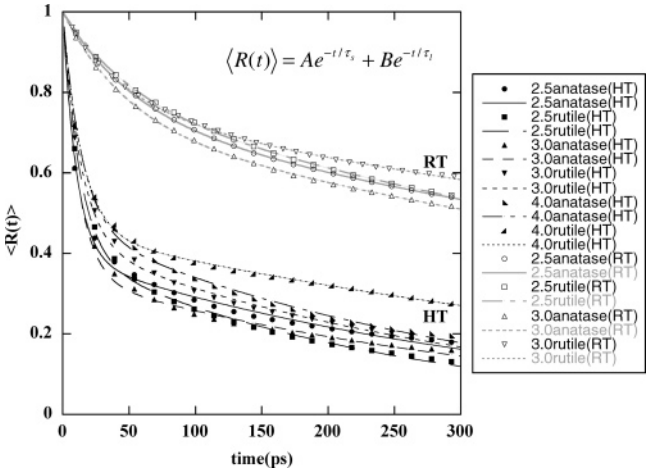

Figure 7. Time correlation function of water molecules at the surface of various sizes of anatase and rutile nanoparticles at hydrothermal conditions (HT) and at ambient conditions (RT). The symbols represent simulation data and the lines are fits to the simulation data as per the fitting parameters listed in Table 5.

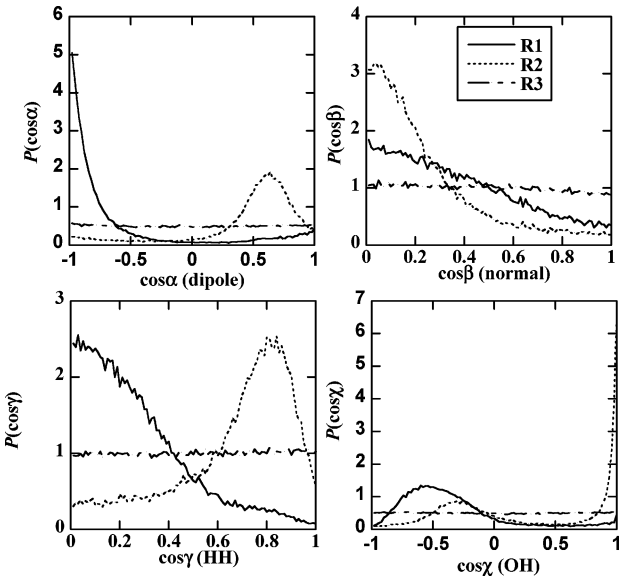

Figure 8. Probability density functions for various water orientations in different regions from the surface of a 3 nm rutile nanoparticle under hydrothermal conditions.

of size, phase, and environmental conditions, three distinct water oxygen peaks are observed around the nanoparticles at 2.1, 2.7, and 4.3 Å, respectively. It is also found that the hydrogen peaks are at 1.7, 2.8, and ~5 Å. It may seem like there are three hydration shells surrounding the nanoparticles. But it is highly improbable for the first two peaks to be separated by a distance of only 0.6 Å between the two. Hence, we believe that there are two hydration shells surrounding the TiO_2 nanoparticles and the water molecules within this first hydration shell interact in two different ways with the nanoparticle surface depending upon the local environment, that is, depending upon whether it is relatively close to a Ti ion or an O ion from the nanoparticle surface. The water molecules in the second hydration shell are far enough from the nanoparticle to indicate any such multiple orientational preferences. To differentiate between the two orientations in the first hydration shell, we have defined different regions on the water distribution profile from the surface. All water molecules with oxygen atoms within the first minima (~2.5 Å) are considered to be in region 1, and all those between the first and the second minima (~3.2 Å) are said to be in region

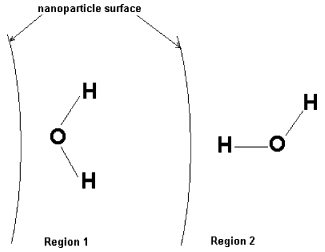

Figure 9. Schematic of the orientational preference of water molecules in regions 1 and 2.

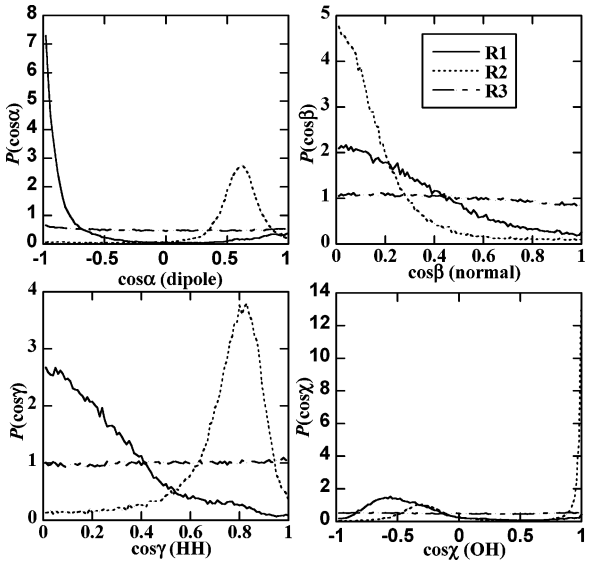

Figure 10. Probability density functions for various water orientations in different regions from the surface of a 3 nm rutile nanoparticle at ambient conditions.

2. All water molecules with oxygen atoms between 3.2 and 5.7 Å from the surface, that is, in the second hydration shell, are considered to be in region 3.

Water Coverage. The solvent accessible surface area of the nanoparticles is calculated for all the simulations by using the method proposed by Meyer.[55] This method is chosen because it is simpler and computationally less intense and yet manages to give results comparable to more complex methods reported in the literature.[56−58] By counting the number of water molecules within the first hydration shell, we can calculate the number of water molecules physically adsorbed on the nanoparticle surface. Knowing the solvent accessible surface area of the nanoparticles, the water coverage is determined and plotted for various nanoparticle diameters in Figure 6. The water coverage increases with increase in particle size for rutile and anatase nanoparticles and is always higher for rutile than anatase suggesting that rutile nanoparticles are slightly more hydrophilic than anatase nanoparticles at all particle sizes and environmental conditions. As the particle size increases, the percentage of Ti ions that are 6-coordinated also increases. Thus the larger particles have a higher percentage of crystallinity than the smaller ones. Also, the curvature of the surface decreases considerably with increase in particle size, tending more and more toward planar surfaces. The coverage is found comparable in magnitude to that of a rutile 110 surface for larger nanoparticles at hydrothermal conditions.

Water Residence Time. To further investigate water adsorption at the metal oxide−nanoparticle surface, we calculated the time correlation function for the water molecules within the first hydration layer from the nanoparticle surface. The residence time correlation function is defined as[59]

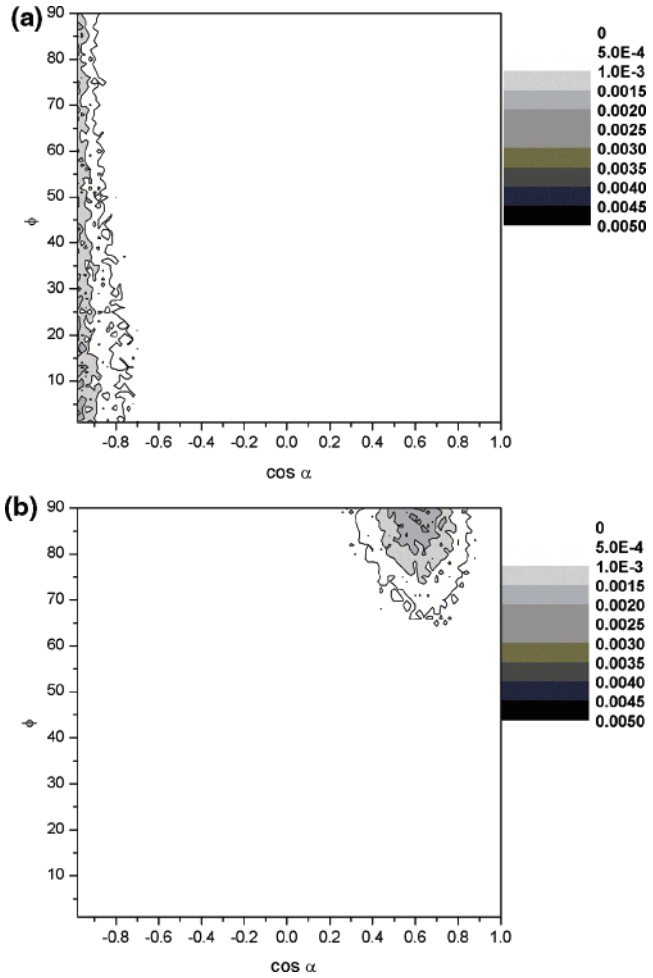

Figure 11. Bivariate distribution plots of a 3 nm rutile nanoparticle under hydrothermal conditions: (a) region 1 and (b) region 2.

$$\langle R(t)\rangle = \left\langle \frac{1}{N_0} \sum_{i=1}^{N_t} \theta_i(0)\, \theta_i(t) \right\rangle \tag{3}$$

where N is the number of water molecules within the first hydration layer from the surface and θ_i is a Heaviside function, which is equal to unity when the molecule i is within the first hydration layer and 0 otherwise. The residence time correlation functions are plotted against simulation time in Figure 7. It is clear that the particle size or phase does not affect the time correlation function significantly but the environmental conditions play a vital role in determining the strength of water adsorption. The residence time can be determined by integrating $\langle R(t)\rangle$

$$\tau = \int_0^\infty \langle R(t)\rangle \tag{4}$$

$\langle R(t)\rangle$ can be expressed as a sum of exponential functions

$$\langle R(t)\rangle = A\mathrm{e}^{-t/\tau_s} + B\mathrm{e}^{-t/\tau_l} \tag{5}$$

where τ_s and τ_l are the short and long residence time constants. The values of the fitted parameters are reported in Table 5 and the functions are also plotted in Figure 7. We integrate eq 5 from 0 to infinity to determine the overall residence time τ, which is reported in Table 5. It is found that water molecules stay at the surface about 5−6 times longer at ambient conditions than at HT.

TABLE 5: Fitting Parameters to Eq 5 and the Overall Integrated Residence Time τ

particle size (nm)	A	B	τ_s (ps)	τ_l (ps)	R	τ (ps)
2.5 anatase (HT)	0.6096 (±0.0074)	0.3904 (±0.0023)	10.35 (±0.21)	340.8(±4.4)	0.996	139.3
2.5 rutile (HT)	0.6028 (±0.0055)	0.3972 (±0.0025)	13.07 (±0.22)	249.1(±2.6)	0.998	106.8
3.0 anatase (HT)	0.6569 (±0.0068)	0.3431 (±0.0024)	11.77 (±0.21)	347.6(±5.3)	0.996	127.0
3.0 rutile (HT)	0.5726 (±0.0057)	0.4274 (±0.0025)	13.89 (±0.25)	320.1(±3.7)	0.997	144.7
4.0 anatase (HT)	0.5312 (±0.0051)	0.4688 (±0.0024)	14.29(±0.25)	309.0(±2.9)	0.998	152.4
4.0 rutile (HT)	0.5492 (±0.0034)	0.4508 (±0.0013)	14.44(±0.16)	586.4(±5.6)	0.999	272.3
2.5 anatase (RT)	0.2584 (±0.0022)	0.7416 (±0.0025)	53.66(±0.76)	907.2(±10.4)	0.999	686.6
2.5 rutile (RT)	0.2194 (±0.0023)	0.7806 (±0.0027)	52.54(±0.94)	796.9(±8.3)	0.999	633.6
3.0 anatase (RT)	0.2804 (±0.0020)	0.7196 (±0.0022)	48.43(±0.63)	897.8(±9.3)	0.999	638.0
3.0 rutile (RT)	0.2467 (±0.0018)	0.7533 (±0.0021)	47.00(±0.69)	1168.6(±15.1)	0.999	891.9

Water Orientation Distribution. The orientation of a water molecule at an interface has frequently been discussed[60] by considering four vectors bound to the water molecule, namely, the dipole vector ($\bar{r}_{dp}$), the normal vector ($\bar{r}_n$), the vector joining the two hydrogen atoms of the water molecule ($\bar{r}_{HH}$), and the vector from the oxygen atom toward any one of the two hydrogen atoms in the water molecule ($\bar{r}_{OH}$). For a planar surface the orientation is characterized by the angles between these four vectors and the vector perpendicular to the planar surface, denoted by the Greek letters α, β, γ, and χ, respectively. To account for the nonplanar nature of the surface under consideration, we redefine these angles as the angles between the four vectors bound to the water molecule ($\bar{r}_{dp}$, $\bar{r}_n$, $\bar{r}_{HH}$, $\bar{r}_{OH}$) and the vector ($\bar{r}_x$) originating from the oxygen atom in the water molecule and normal to the triangle ABC, formed by the three surface ions nearest to the water molecule under consideration. It should be noted that the vectors $\bar{r}_n$ and $\bar{r}_{HH}$ can be equally directed in two opposite directions unlike the vectors $\bar{r}_{dp}$ and $\bar{r}_{OH}$, and there is no physical way of distinguishing between them. Hence, the angles β and γ can only vary between 0° and 90°, while the angle α and χ varies between 0° and 180°. To determine the orientational preference of the water molecules, we determine the probability density functions of the cosines of the angles α, β, γ, and χ in the regions 1, 2, and 3. cos β and cos γ will lie between 0 and 1, and cos α and cos χ will vary between −1 and 1.

Figure 8 shows these probability density functions for a 3 nm rutile at HT. It is found that all probability density functions show similar trends at all phases and sizes at HT.

Region 1. In this region the most preferred values of α, β, γ, and χ are 180°, 90°, 90°, and 127°, respectively. This indicates that the water molecules in this region are aligned in such a way that their dipole moment vector is almost parallel to the surface normal, with the oxygen being close to the surface and hydrogen atoms oriented away. The $\bar{r}_{HH}$ vector is also perpendicular to the surface normal confirming this arrangement. Thus, the region 1 comprises the water molecules that are interacting with the Ti ions on the nanoparticle surface. The schematic in Figure 9 gives a better interpretation of this orientation.

Region 2. In region 2, α, β, and γ have the highest probability for the values 53°, 90°, and 35°. The angle with the $\bar{r}_{OH}$ vector has high probabilities for two angles, namely, 0° and 109°. This indicates that the water molecules in region 2 have one of their $\bar{r}_{OH}$ vectors aligned pointing toward the surface, parallel but in the opposite direction of the surface normal. The plane of the molecules is preferentially perpendicular to the surface. This is depicted as a schematic in Figure 9.

Region 3. The probability density functions for all angles are almost flat in region 3 inferring that there is no preferential orientation of the water molecules in this region, thereby indicating bulk-like behavior.

The probability density functions at ambient conditions are shown in Figure 10. They indicate that at room temperature and pressure, the peaks get narrower and taller but their positions remain unchanged, indicating that the orientations at ambient conditions are similar to HT in the various regions but the preference of these orientations over other possible ones is greatly increased.

Bivariate Plots. Although the above-mentioned probability distribution functions give us information about the preferential orientation of a single water molecule, their joint statistical distribution cannot be obtained from their individual distribution due to the fact that these angles are not mutually independent. For example, angles α and β can have some preferential values but we cannot say with certainty that these values appear simultaneously. Hence, to get independent molecular directions we define a new angle ϕ as the angle between the vector $\bar{r}_n$ with the projection of the vector $\bar{r}_x$ in the plane containing the vectors $\bar{r}_n$ and $\bar{r}_{HH}$. The vectors $\bar{r}_{dp}$, $\bar{r}_{HH}$, and $\bar{r}_n$ define the frame of reference. Uniform spatial distribution of water molecules in bulk water would lead to uniform distribution of the angle ϕ and the cosine of the angle α. Hence, the joint probability distribution of ϕ and cos α would provide us information on molecular orientation with greater certainty. These $P(\cos\alpha,\phi)$ plots are referred to as bivariate distribution plots. We determined the bivariate distributions in regions 1 and 2 for simulations at HT and these are reported in Figure 11.

In region 3, the distribution of water molecules is indeed uniformly random as a uniform bivariate distribution was obtained. In region 1, the water molecules exhibit a strong preference for a value of 180° for α. The plot of region 2 shows that there is an orientational preference in this region for α and ϕ to be 53° and 90°, respectively. This means that water molecules are aligned with one of their hydrogen atoms pointed toward the surface with the $\bar{r}_{OH}$ perpendicular to the surface and the molecular normal being parallel to the surface.

Conclusions

This research work investigated the adsorption of molecular water on the surfaces of anatase and rutile nanoparticles. It was found that the rutile nanoparticles were more hydrophilic than anatase nanoparticles of the same size, both at room temperature (T = 300 K, P = 1 bar) and under hydrothermal conditions (T = 523 K, P = 50 kbar). When nanoparticles are inserted in water, they undergo structural modification but no phase transformation occurs over the time scales accessible via molecular dynamics simulations. As a result of this modification, we do observe phase enhancement or greater crystallinity. This is indicated by a higher percentage of 6-coordinated Ti ions in the nanoparticle in water and taller/narrower peaks in the simulated X-ray diffraction pattern. The number of water molecules per unit surface area of the nanoparticles (coverage) increased with the size of the nanoparticles and with the percentage crystallinity of the particle. The coverage for rutile is always greater than that for the anatase nanoparticle of the

same size, corroborating our previous conclusion. Also, the water molecules reside ~5−6 times longer on the nanoparticle surface at room temperature than under hydrothermal conditions.

By careful examination of the results, we can conclude that there are two hydration layers present around the nanoparticles. The first hydration layer has water molecules with two distinctly different orientation preferences. No such orientational preference is observed in the second hydration layer. The interactions between the water molecules in the first hydration layer and the nanoparticle surface are dependent on the local environment of the water molecule under consideration, that is, its proximity to a Ti or O surface ion. The bivariate plots also depict the probabilistic preferences of these two orientations.

Acknowledgment. We would like to acknowledge the National Science Foundation (EAR- 0308539) for the funding for this work and the National Energy Research Scientific Computing Center for providing computer time to run the simulations. We also express our thanks to an anonymous reviewer, whose careful criticism of an earlier version of this paper has resulted in considerable improvement.

References and Notes

(1) Dewdney, A. K. *Sci. Am.* **1988**, *258*, 100.
(2) Franks, A. *J. Phys. E*: *Sci. Instrum.* **1987**, *20*, 1442.
(3) Siegel, R. W. *Phys. Today* **1993**, *46*, 64.
(4) Siegel, R. W.; Sanders, P. G.; Witney, A. B.; Weertman, J. R. *Mater. Sci. Eng. A* **1995**, *204*, 7.
(5) Tsukagoshi, K.; Yoneya, N.; Uryu, S.; Aoyagi, Y.; Kanda, A.; Ootuka, Y.; Alphenaar, B. W. *Phys. B* **2002**, *323*, 107.
(6) Laurvick, C. A.; Singaraju, B. *IEEE Aerospace Electron. Syst. Magazine* **2003**, *18*, 18.
(7) Gooding, J. J. *Electrochim. Acta* **2005**, *50*, 3049.
(8) Sahoo, S. K.; Labhasetwar, V. *Drug Discovery Today* **2003**, *8*, 1112.
(9) Silva, G. A. *Surg. Neurol.* **2004**, *61*, 216.
(10) Akhtar, M. K.; Yun, X. O.; Pratsinis, S. E. *AIChE J.* **1991**, *37*, 1561.
(11) Collins, D. R.; Smith, D. J.; Harrison, N. M.; Forester, T. R. *J. Mater. Chem.* **1997**, *7*, 2543.
(12) Collins, D. R.; Smith, W.; Harrison, N. M.; Forester, T. R. *J. Mater. Chem.* **1996**, *6*, 1385.
(13) Kolen'ko, Y. V.; Burukhin, A. A.; Churagulov, B. R.; Oleynikov, N. N. *Mater. Lett.* **2003**, *57*, 1124.
(14) Zhang, H.; Banfield, J. F. *J. Mater. Chem.* **1998**, *8*, 2073.
(15) Ding, X. Z.; Liu, X. H. *J. Alloys Compd.* **1997**, *248*, 143.
(16) Ohtani, B.; Okugawa, Y.; Nishimoto, S.; Kagiya, T. *J. Phys. Chem.* **1987**, *91*, 3550.
(17) Martin, S. T.; Lee, A. T.; Hoffmann, M. R. *Environ. Sci. Technol.* **1995**, *29*, 2567.
(18) Augugliaro, V.; Loddo, V.; Palmisano, L.; Schiavello, M. *J. Catal.* **1995**, *153*, 32.
(19) Fox, M. A.; Dulay, M. T. *Chem. Rev.* **1993**, *93*, 341.
(20) Hotsenpiller, P. A. M.; Bolt, J. D.; Farneth, W. E.; Lowekamp, J. B.; Rohrer, G. S. *J. Phys. Chem. B* **1998**, *102*, 3216.
(21) Fujihira, M.; Satoh, Y.; Osa, T. *Nature* **1981**, *293*, 206.
(22) Gruy, F.; Pijolat, M. *J. Am. Ceram. Soc.* **1992**, *75*, 657.
(23) Banfield, J. F.; Veblen, D. R.; Smith, D. J. *Am. Mineral.* **1991**, *76*, 343.
(24) Hu, Y.; Tsai, H. L.; Huang, C. L. *J. Eur. Ceram. Soc.* **2003**, *23*, 691.
(25) Freeman, C. M.; Newsam, J. M.; Levine, S. W.; Catlow, C. R. A. *J. Mater. Chem.* **1993**, *3*, 531.
(26) Ding, X. Z.; Liu, X. H. *J. Mater. Res.* **1998**, *13*, 2556.
(27) Cheng, H.; Ma, J.; Zhao, Z.; Qi, L. *Chem. Mater.* **1995**, *7*, 663.
(28) Yang, J.; Mei, S.; Ferreira, J. M. F. *J. Mater. Res.* **2002**, *17*, 2197.
(29) Ovenstone, J. *J. Mater. Sci.* **2001**, *36*, 1325.
(30) Kobata, A.; Kusakabe, K.; Morooka, S. *AIChE J.* **1991**, *37*, 347.
(31) Stark, W. J.; Pratsinis, S. E. *Powder Technol.* **2002**, *126*, 103.
(32) Pratsinis, S. E.; Spicer, P. T. *Chem. Eng. Sci.* **1998**, *53*, 1861.
(33) Yin, S.; Li, R. X.; He, Q. L.; Sato, T. *Mater. Chem. Phys.* **2002**, *75*, 76.
(34) Swamy, V.; Gale, J. D. *Phys. Rev. B* **2000**, *62*, 5406.
(35) Sawatari, H.; Iguchi, E.; Tilley, R. J. D. *J. Phys. Chem. Solids* **1982**, *43*, 1147.
(36) Roux, H. L.; Glasser, L. *J. Mater. Chem.* **1997**, *7*, 843.
(37) Post, J. E.; Burnham, C. W. *Am. Mineral.* **1986**, *71*, 142.
(38) Oliver, P. M.; Watson, G. W.; Kelsey, E. T.; Parker, S. C. *J. Mater. Chem.* **1997**, *7*, 563.
(39) Mostoller, M.; Wang, J. C. *Phys. Rev. B* **1985**, *32*, 6773.
(40) Matsui, M.; Akaogi, M. *Mol. Simul.* **1991**, *6*, 239.
(41) Kim, D. W.; Enomoto, N.; Nakagawa, Z.; Kawamura, K. *J. Am. Ceram. Soc.* **1996**, *79*, 1095.
(42) Catlow, C. R. A.; James, R. *Proc. R. Soc. London, Ser. A* **1982**, *384*, 157.
(43) Catlow, C. R. A.; Freeman, C. M.; Royal, R. L. *Phys. B* **1985**, *131*, 1.
(44) Collins, D. R.; Smith, W. Council for the Central Laboratory of Research Councils, Daresbury, 1996; Research Report DL-TR-96−001.
(45) Swamy, V.; Gale, J. D.; Dubrovinsky, L. S. *J. Phys. Chem. Solids* **2001**, *62*, 887.
(46) Bandura, A. V.; Kubicki, J. D. *J. Phys. Chem. B* **2003**, *107*, 11072.
(47) Naicker, P. K.; Cummings, P. T.; Zhang, H. Z.; Banfield, J. F. *J. Phys. Chem. B* **2005**, *109*, 15243.
(48) Berendsen, H. J. C.; Grigera, J. R.; Straatsma, T. P. *J. Phys. Chem.* **1987**, *91*, 6269.
(49) Smith, W.; Forester, T. R. *J. Mol. Graphics* **1996**, *14*, 136.
(50) Smith, W. *J. Mol. Graphics* **1987**, *5*, 71.
(51) Koparde, V. N.; Cummings, P. T. *J. Phys. Chem. B* **2005**, *109*, 24280.
(52) Kazakov, A. V.; Shpiro, E. S.; Voskoboinikov, T. V. *J. Phys. Chem.* **1995**, *99*, 8323.
(53) Zhang, H. Z.; Gilbert, B.; Huang, F.; Banfield, J. F. *Nature* **2003**, *424*, 1025.
(54) Predota, M.; Bandura, A. V.; Cummings, P. T.; Kubicki, J. D.; Wesolowski, D. J.; Chialvo, A. A.; Machesky, M. L. *J. Phys. Chem. B* **2004**, *108*, 12049.
(55) Meyer, A. Y. *J. Comput. Chem.* **1988**, *9*, 18.
(56) Perrot, G.; Cheng, B.; Gibson, K. D.; Vila, J.; Palmer, K. A.; Nayeem, A.; Maigret, B.; Scheraga, H. A. *J. Comput. Chem.* **1992**, *13*, 1.
(57) Legrand, S. M.; Merz, K. M. *J. Comput. Chem.* **1993**, *14*, 349.
(58) Gavezzotti, A. *J. Am. Chem. Soc.* **1985**, *107*, 962.
(59) Impey, R. W.; Madden, P. A.; McDonald, I. R. *J. Phys. Chem.* **1983**, *87*, 5071.
(60) Jedlovszky, P.; Vincze, A.; Horvai, G. *J. Chem. Phys.* **2002**, *117*, 2271.